Thermo-Optic Designs for Electromagnetic-Field Probes for Microwaves and Millimeter Waves

James Randa, *Member, IEEE,* Motohisa Kanda, *Fellow, IEEE,* and R. David Orr

Abstract—**We report the development of an electromagnetic-field probe for microwave and millimeter-wave frequencies. The probe uses an optically sensed thermometer to measure the heating of a resistive element in an electromagnetic field. The response is calculated for several different configurations of the resistive element, and two optimal designs are chosen. Measurements on experimental probes of these designs are presented. One of the designs displays a flat frequency response above 30 GHz and a sensitivity of 38 V/m. We identify improvements in the design that should significantly increase the sensitivity and improve the low-frequency response.**

I. Introduction

THERE IS A growing need for basic measurement support for millimeter wave and upper microwave frequencies. One part of the metrology infrastructure that requires development is transfer standard probes, which are electric (or magnetic) field probes used to compare standard electromagnetic fields generated in different calibration laboratories. A related area that also needs development is that of radiation hazard meters. In principle, there is no reason the same probe could not serve both purposes. The requirements for the two applications are different but not mutually exclusive. A transfer standard is used in a calibration laboratory, where the premium is on accuracy and repeatability—high performance under controlled conditions. Measurements in the field, on the other hand, require more durability and portability than in the lab, but they can typically afford somewhat less accuracy. Thus, although our primary interest is the development of a transfer standard probe, we shall also devote some attention to properties required by a radiation hazard probe. Besides durability and portability, these include isotropy, flat frequency response, and ability to handle complex fields (multiple frequencies, near fields, etc.).

At present, transfer standard probes developed and used by the National Institute of Standards and Technology (NIST) operate at frequencies up to 18 GHz [1]. There is a need to extend this range up to 110 GHz, and two approaches are being pursued to try to fill this need. One approach is to modify the 18-GHz design for use at higher frequencies. This design consists of a resistively tapered, thin-film dipole with a diode detector and resistive leads. By using shorter dipoles, we hope to extend the operating range of this design to 35 or 40 GHz. The resistively tapered dipole effort will be reported elsewhere [2]. This paper is devoted to the second approach, which uses an optically sensed thermometer to measure the temperature rise of a resistive element in an electromagnetic field. We shall refer to this as the thermo-optic (TO) design. An earlier, condensed account of this work can be found in [3]. In this paper, we shall present calculations of the sensitivities and frequency responses for various choices of the resistive element of the probe. Results of measurements on probe tips of a particular design will also be presented.

All the TO designs we consider share certain features, some of which are common to other resistive designs as well [1], [4]–[6]. Because the sensing element is very resistive, the half-wave resonance is suppressed, resulting in a flat response over a wide frequency band. The probes are all quite small, which allows good spatial resolution. The smallness and high resistivity are also major factors in the nonperturbing feature of the probe; very little power is scattered by the sensing element or by the optical fiber used to convey the signal to the metering unit. In addition, the optical fiber should not itself pick up any stray signals, which is a significant problem for electrically sensed probes at millimeter wave frequencies. Because the basic temperature sensor can measure temperatures of several hundred degrees Celsius, very high field levels can be measured. A final attractive feature of the TO designs is that they are directly sensitive to the average electric (and/or magnetic) field squared. They are therefore not subject to the multiple-frequency problems that can beset probes using a diode detector [7].

There is, of course, a price to be paid for these desirable features. The major obstacle in developing a probe of the TO design is achieving sufficient sensitivity. We have adopted the goal of about 60 V/m for a minimum detectable electric field (an equivalent plane wave power density of 1 mW/cm^2), and some of the designs do not achieve even this rather modest goal. Response time is another traditional problem area for thermally sensed probes. For transfer standards, the problem is not so severe. The TO designs considered in this paper have response times of order 1 min. That is quite acceptable for a transfer standard, but it would be too slow for certain applications involving transient or pulsed fields. Thermal stability is another potential problem that must be addressed. Short-term instabilities caused by drafts and the like can be (and are) eliminated by enclosing the sensing element in a box or protective shield. The problem of long-term thermal drift must also be eliminated. For this purpose, a second temperature sensor is included in all the designs to measure the ambient temperature. By taking the difference between

Manuscript received May 17, 1990; revised February 12, 1991. This work was supported by the Naval Ocean Systems Center, San Diego, CA, under contract N6600190MP00018.

The authors are with the Electromagnetic Fields Division, National Institute of Standards and Technology, Boulder, CO 80303.

IEEE Log Number 9144863.

the active and the ambient temperature sensors, we hope to eliminate the effects of ambient heating and minimize the problem of thermal drift.

The next section contains background information, a description of the optically sensed thermometer around which the TO designs are built, and an overview of the five different choices considered for the resistive element of the probe. Section III is devoted to the computation of the sensitivity and frequency response for each of the different choices for the resistive element. The fourth section gives details and results of measurements made on probe tips of two particular designs, and the final section comprises comments and a summary.

II. Basic Design

The TO designs are all built around a commercially available optically sensed thermometer. We only summarize relevant features of its operation here; interested readers are referred to [8] for further details. The temperature sensor is based on the property of certain fluorescent phosphors that the lifetimes of their excited states are temperature dependent. Therefore, by exciting such a phosphor and then measuring its decay time, one can measure the temperature of the phosphor and consequently of anything with which it is in thermal equilibrium. In the commercial version of the temperature sensor, a small quantity (about 40 μg) of a phosphor is attached to the end of an optical fiber by a clear bonding agent. The phosphor is excited by a pulse of light carried by the fiber, and the light emitted by the phosphor as it decays is carried back down the same fiber to be measured to determine the decay time. The temperature sensor can be used in either of two configurations: either with the phosphor attached to the fiber as just described or with a phosphor paste smeared on the surface of the object whose temperature is to be measured and with the phosphor viewed by the fiber from a (very small) distance.

To turn this temperature sensor into an electric-field probe, we simply introduce a resistive element that will undergo Joule heating due to the current induced in the element when it is placed in an electromagnetic field. The feasibility of this approach was first demonstrated in [9], where the resistive element consisted of crossed dipoles of carbon painted onto a piece of styrofoam. The temperature sensor was then sandwiched between this and another piece of styrofoam with the phosphor tip located at the intersection of the two dipoles.

The configurations we have considered for the resistive element are shown in Fig. 1. The first consists of a thin rectangular resistive strip deposited directly on the phosphor tip of the temperature sensor. The end of the fiber is cut at an oblique angle to increase the size of the strip that can be deposited. This configuration will be called the patch tip design. Fig. 1(b) is the suspended patch design in which a thin substrate is fashioned from a phosphorescent material. A rectangular resistive strip is deposited on the substrate, which is viewed remotely. (The substrate is supported by some unspecified means that is assumed to conduct negligible heat.) The advantage of this design over the patch tip design of Fig. 1(a) is that the phosphor is thermally insulated from

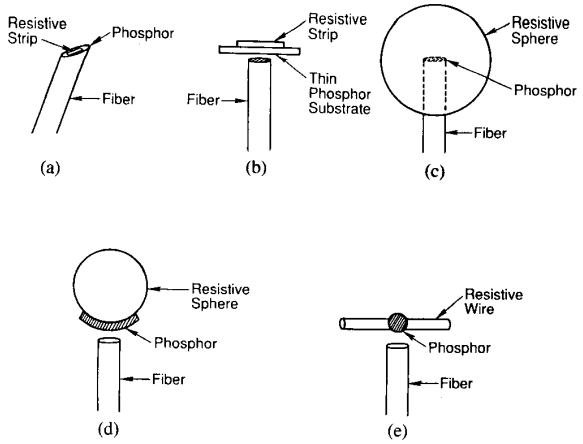

Fig. 1. Different TO probe designs considered in this paper: (a) Patch tip; (b) suspended patch; (c) sphere tip; (d) suspended sphere; (e) suspended wire.

the optical fiber. The rate of heat loss should therefore be less, and the temperature rise of the phosphor should be correspondingly greater. Just how big the effect is will be seen in the calculation of the next section. The disadvantage of the suspended patch design relative to the patch tip design lies in the difficulty of fabrication. Besides the problem of supporting the substrate, a suitable phosphor substrate would itself require some development.

The third configuration is the resistive sphere tip design of Fig. 1(c). A solid resistive sphere is formed around the phosphor tip. If the sphere is sufficiently resistive, the field can permeate the entire volume. When the entire volume is heated in this manner, much more power can be absorbed than with the thin strips in the first two designs. On the other hand, this design suffers from the thermal contact between the phosphor and the optical fiber, which constitutes a significant heat sink. The suspended sphere design (Fig. 1(d)) eliminates the heat sink problem by suspending the sphere above the fiber. The side of the sphere facing the fiber is coated with the phosphor paste. The final design is the suspended wire of Fig. 1(e). It is similar to the suspended sphere except that a thin solid cylinder is substituted for the sphere. In both cases, the material is sufficiently resistive that the field penetrates the entire volume.

The responses of these five TO designs have been calculated. We present one of the calculations, outline the others, and compare the results in the next section. The calculations involve three steps: the electromagnetic problem of calculating the power absorbed for a given incident field, the thermal problem of calculating the temperature rise of the phosphor for a given absorbed power, and variation of the free parameters to maximize the temperature rise of the phosphor for a given incident field. Several simplifying assumptions will be made, and some of the electromagnetic and thermal properties of the materials are not known very well. Consequently, the calculation results are not to be considered actual theoretical predictions but rather estimates of the expected responses to be used as guides in choosing the optimal probe design.

III. Calculation

A. Resistive Sphere Designs

The two probe designs that prove to be the most promising both use a resistive sphere as the resistive element—either surrounding the phosphor tip of the temperature sensor, as in Fig. 1(c) (sphere tip design), or suspended above the fiber with the phosphor paste on the underside of the sphere viewed remotely by the fiber, as in Fig. 1(d) (suspended sphere design). The suspended sphere configuration has the advantage that the resistive element is not in thermal contact with the fiber and thus loses heat only to the air (provided that the suspension mechanism transfers negligible heat). It should therefore be more sensitive than the sphere tip configuration, but the sphere tip is considerably easier to fabricate. An advantage shared by both resistive sphere designs is that for low enough conductivity, the field can penetrate into the interior of the sphere, and heat is generated throughout the sphere's volume. Far more power is absorbed in this case than when only a surface current is generated—as is effectively the case for a thin conductive strip or a sphere of high enough conductivity that the induced current is confined to a thin shell at the surface.

Calculation of the response of the probe to an incident electromagnetic field is broken into two parts: the electromagnetic problem of calculating the absorbed power and the thermal problem of calculating the temperature rise for a given absorbed power. For calculation of the power absorbed in an electromagnetic field, we treat the resistive structure as a solid homogeneous sphere of resistive material for both configurations (sphere tip and suspended sphere). This is certainly an approximation for the sphere tip configuration since in that case, the optical fiber extends into the center of the sphere, where the phosphor is located. It is probably a very good approximation for the suspended sphere configuration since the suspension mechanism is likely to be some sort of very thin thread through the sphere. The power absorbed by the resistive sphere of radius r can be obtained from the classic Mie results [10], which are reproduced in standard texts, such as [11] and [12]. The absorption cross section is given by the difference between the total cross section and the scattering cross section

$$\sigma_{\text{abs}} = \sigma_{\text{tot}} - \sigma_{\text{sc}}$$

$$\sigma_{\text{tot}} = \frac{2\pi}{k_1^2} \sum_{n=1}^{\infty} (2n+1)\,\text{Re}\{a_n^r + b_n^r\}$$

$$\sigma_{\text{sc}} = \frac{2\pi}{k_1^2} \sum_{n=1}^{\infty} (2n+1)\{|a_n^r|^2 + |b_n^r|^2\} \tag{1}$$

where

$$a_n^r = \frac{\mu_2 j_n(N\rho)\left[\rho j_n(\rho)\right]' - \mu_1 j_n(\rho)\left[N\rho j_n(N\rho)\right]'}{\mu_2 j_n(N\rho)\left[\rho h_n^{(1)}(\rho)\right]' - \mu_1 h_n^{(1)}(\rho)\left[N\rho j_n(N\rho)\right]'}$$

$$b_n^r = \frac{\mu_2 j_n(\rho)\left[N\rho j_n(N\rho)\right]' - \mu_1 N^2 j_n(N\rho)\left[\rho j_n(\rho)\right]'}{\mu_2 h_n^{(1)}(\rho)\left[N\rho j_n(N\rho)\right]' - \mu_1 N^2 j_n(N\rho)\left[\rho h_n^{(1)}(\rho)\right]'} \tag{2}$$

$$N = k_2/k_1,\ \rho = k_1 r.$$

The prime indicates a derivative with respect to the argument of the Bessel or Hankel function in the bracket. The subscripts 1 and 2 refer to the surrounding medium and the sphere, respectively, k is the (complex) wavenumber, and $j_n(h_n)$ is the nth-order spherical Bessel (Hankel) function. The absorbed (scattered) power is obtained by multiplying $\sigma_{\text{abs}}(\sigma_{\text{sc}})$ by the incident power density (dP/dA)

$$P_{\text{abs}} = \sigma \times \frac{dP_{\text{inc}}}{dA}. \tag{3}$$

Unlike the thin-strip and wire designs considered below, the resistive sphere has significant response to both electric and magnetic fields in the range of frequencies and parameters we consider. This is acceptable for transfer standards since such use typically involves an incident plane wave with a known ratio of E to H. For hazard meter or other near-field applications, however, further study and characterization would be required.

The rate at which heat is lost to the surrounding air is given by

$$P_{\text{air}} = 4\pi r^2 h \Delta T \tag{4}$$

where r is the radius of the sphere, ΔT is the temperature difference between sphere and air, and a typical value for the constant h is 10 W/(°C m^2) for still air [13]. If the sphere is attached to the optical fiber, as in Fig. 1(c), then heat is also lost to the fiber at a rate (P_f) proportional to the temperature gradient normal to the sphere surface, integrated over the area of the sphere-fiber interface (if the fiber were just attached to the outside of the sphere). As an approximation we use

$$P_f = k_f(\pi R^2)(\Delta T/R) \tag{5}$$

where R is the fiber radius, and k_f is its thermal conductivity. The temperature rise of the sphere in the steady state is then determined by equating the rate of heat loss to the power absorbed, yielding

$$\Delta T = P_{\text{abs}}/(4\pi r^2 h + \pi R k_f) \tag{6}$$

for the spherical tip on the fiber and

$$\Delta T = P_{\text{abs}}/(4\pi r^2 h) \tag{7}$$

for the suspended sphere.

We then vary the sphere radius and conductivity to maximize ΔT. The fiber radius R and thermal conductivity k_f are held fixed at 0.21 mm and 0.76 W/(°C m), respectively. Plots of ΔT versus frequency for $\sigma = 10$ S/m and various radii are given in Fig. 2 for the suspended sphere case. Based on these and other plots, we chose the optimal conductivity and radius to be $\sigma = 10$ S/m, $r = 2$ mm. With these values and a minimum detectable temperature rise of 0.04°C, the minimum detectable electric field is predicted to be 21 V/m, which is much better than our minimal design goal of about 61 V/m. The sensitivity could be increased slightly by using a smaller radius; however, the lower cut-off frequency would

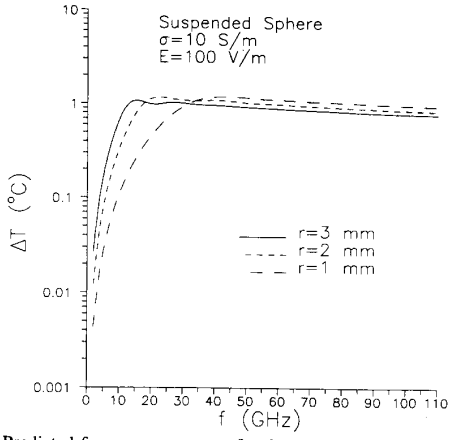

Fig. 2. Predicted frequency response for the suspended sphere design with 10 S/m conductivity.

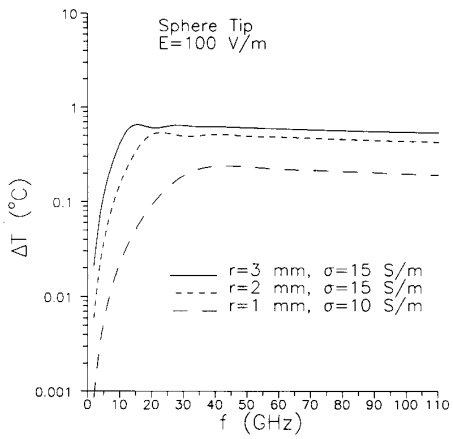

Fig. 3. Predicted frequency response for the sphere tip design for various radii and conductivities.

be raised considerably by doing so. For the case of the spherical tip on the fiber, the optimization results are different due to the different r dependence of the rate of heat loss. The predicted frequency responses for selected r, σ are shown in Fig. 3. Optimal values are found to be $\sigma = 15$ S/m, $r = 3$ mm, and they result in a minimum detectable electric field of $E = 27$ V/m. This represents a decrease in sensitivity relative to the suspended sphere design, but it is still sensitive enough to meet our nominal design criterion. In comparing the two resistive sphere designs, we should remember that their relative sensitivities are quite dependent on the thermal constants h and k_f, which we have only estimated, and on the simplifying assumption that the sphere surrounding the fiber tip can be treated as a solid homogeneous sphere.

B. Other Designs

Detailed calculations were also performed for the other three designs of Fig. 1. In order to save space and because these designs were not pursued further, we only summarize the calculations and results here.

The first two designs of Fig. 1 are both based on a resistive element consisting of a thin resistive strip. The patch tip design of Fig. 1(a) consists of a thin film of resistive material deposited on the phosphor or on the phosphor and fiber. Initial calculations led us to choose a thin rectangular strip deposited on an inclined phosphor tip, as opposed, for example, to a strip on a flat phosphor or a thin resistive cylinder around the phosphor and fiber. The second TO design consists of a thin rectangular resistive strip deposited on a thin substrate of fluorescent material. This phosphor substrate is then viewed remotely (at a distance of about 25 μm) by the fiber, as is depicted in Fig. 1(b). We refer to this design as the suspended patch design. The electromagnetic aspects are similar for these two designs, and we treat them together for the electromagnetic part of the calculation.

The power absorbed by a resistive strip is calculated by integrating the induced current density squared times the resistivity over the volume of the strip. The thickness of the thin strip will be significantly less than the skin depth; therefore, the current density does not vary appreciably with depth into the strip. We assume a sinusoidal current distribution in the longitudinal direction and no variation in the transverse direction. The incident field is assumed to be constant across the length and width of the strip. In addition, we calculate the induced current for a strip in free space, neglecting the effect of the dielectric on which the strip is deposited. For the suspended patch configuration, this is a good approximation because the substrate is electrically thin. For the patch tip design, it will lead to an overestimate of the response, and that will be sufficient for our purpose. The normalization of the current distribution is calculated by treating the strip as a short-circuit receiving dipole. The midpoint current is then given by $I(0) = E_z L_{eff}/Z_{in}$, where L_{eff} is the effective length, and Z_{in} is the input impedance of the dipole used in the transmitting mode. The effective length of a sinusoidal current distribution is well known. The input impedance is given by the sum of the input impedance for a perfectly conducting dipole of the same shape plus a contribution due to the finite conductivity. The contribution due to the finite conductivity is primarily resistive and is easily determined from the resistivity and geometry. The input impedance for a perfectly conducting strip dipole is estimated by treating it as having a highly eccentric elliptical cross section [14] so that the total current and, therefore, the input impedance can be related to those of a cylindrical dipole of circular cross section with the appropriate effective radius [15]. Since the input impedance of a circular cylindrical dipole is well known [16], this is sufficient to determine the midpoint current and, therefore, the power absorbed by the strip.

The next step is to relate the temperature rise of the phosphor to the absorbed power. For the temperature rises we encounter, radiative heat transfer is negligible. For the patch tip, the principal mechanism for heat transfer is conduction from the strip to the phosphor and then to the optical fiber, whereas for the suspended patch design, the heat is conducted from the strip to the phosphor substrate and then is lost to the air by both strip and substrate.

Considering the patch tip first, the following approximations were made: the phosphor was taken to be a circular

cylinder, the strip was assumed to cover the top surface of the phosphor, the bottom surface of the phosphor was held at ambient temperature, and all the heat absorbed by the strip was transferred to the phosphor. (These approximations lead to an overestimate of the temperature rise.) The temperature rise of the phosphor can then be written in terms of the absorbed power, the area covered by the strip, the thermal conductivity of the phosphor [measured to be 0.81 W/(°C · m)], and known mathematical functions. Once we have an expression for the temperature rise of the phosphor for a given incident field, we can vary the physical parameters (length, thickness, and conductivity of strip) to maximize the temperature rise and, therefore, the sensitivity. An analytic expression can be obtained for the optimal value of the surface resistivity $(1/\sigma t)$, but that value is frequency dependent. The choice of frequency at which σt is optimized affects not only the sensitivity but the frequency response of the probe as well. (We refer to this optimization frequency as f_{opt} and emphasize that it is an "optimization" frequency and not an "optimal" frequency.) The same is true of the length of the strip L. To investigate the tradeoffs involved, we computed and plotted $\langle \Delta T_{ph} \rangle$ as a function of frequency for various choices of L and f_{opt} (or equivalently σt). In all cases, the strip width was taken to be $L/4$, which is the largest value that still gave a good suppression of cross-polarization response. Fig. 4 shows the predicted temperature rise (above ambient) for a 100-V/m field as a function of frequency for $L = 2$ mm and various values of $f_{opt}(\sigma t)$. There is a tradeoff between peak sensitivity, which is maximum for large f_{opt}, and frequency response, which is flattest for small f_{opt}. An optimization frequency of 20 GHz yields the greatest sensitivity while still retaining an acceptable frequency dependence. In a similar manner, optimal optimization frequencies were found for other strip lengths, and these results were then compared. On the basis of that comparison, we chose $L = 2$ mm and $f_{opt} = 20$ GHz $(1/\sigma t = 209\ \Omega)$ for the optimum values. For these values, the temperature rise in a 100 V/m field is about 0.003°C for frequencies above about 22 GHz. We shall see below that we can detect temperature rises of 0.04°C and larger. As can be seen from the figures, even with all parameters optimized, the patch tip design is too insensitive to be of use. We estimate that the minimum detectable field with this design would be about 365 V/m (35.3 mW/cm^2).

For the suspended patch design, the rate of heat loss will depend on the thickness of the phosphor substrate. For a very thin substrate (much thinner than 4 μm), the heat conducted out to the uncovered part of the substrate can be neglected, and heat is lost to the air only by the surface of the resistive strip and that portion of the bottom surface of the substrate that is directly below the strip. For thicker substrates, appreciable heat is conducted out to the uncovered part of the substrate, which in turn loses heat to the air. This results in a smaller temperature rise: a factor of about 0.4 times that for a very thin substrate. In either case, optimization of the response is much the same as for the patch tip design treated above. P_{abs} is the same in both cases, and in both cases, the temperature rise of the phosphor is inversely proportional to the area of the strip. As a result, the optimal dimensions and conductivity are again found to be $L = 2$ mm and $1/\sigma t = 209\ \Omega$. The curve giving the response as a function of frequency then has the same shape as for the patch tip (Fig. 4), but the normalization is different. The response for a very thin ($\ll 4$ μm) phosphor substrate is about 220 times that for the patch tip, and for a thicker phosphor, it is about 90 times that for the patch tip. The minimum detectable electric field is thus 25 V/m (39 V/m for a thicker substrate). The normalized curve for the suspended patch design will be shown in the comparison of the different designs at the end of this section.

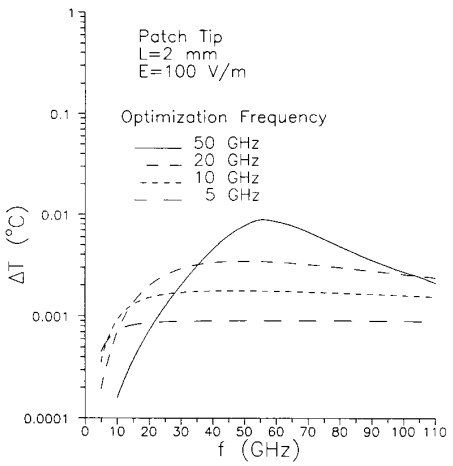

Fig. 4. Predicted frequency response for patch tip design with $L = 2$ mm, $w = 0.5$ mm, and various optimization frequencies.

The final configuration we consider for the resistive element is the resistive wire design depicted in Fig. 1(e). The wire has a small amount of phosphor attached at the midpoint and is suspended above the fiber that views the phosphor. The calculation of the power absorbed by the wire is similar to that for the thin strip, except that the current density is not uniform across the cross section of the wire. Instead, it varies with distance from the wire axis as a zero-order Bessel function. Again, the longitudinal dependence of the current distribution is assumed to be sinusoidal; therefore, L_{eff} is the same as for the thin strip. Similarly the input impedance comprises the usual impedance of a perfectly conducting cylindrical dipole plus a calculable contribution due to the finite conductivity. An expression for the absorbed power can then be obtained, though it does contain an integral that must be evaluated numerically. The heat is lost to the air; therefore, the equilibrium temperature rise is just the absorbed power divided by the surface area times a constant. As above, we varied the wire dimensions (length L and radius a) and conductivity to optimize the response as a function of frequency. The optimal values are found to be about $L = 2$ mm, $a = 0.143$ mm, and $\sigma = 30$ S/m. A plot of the response for these values will be shown in the comparison below. The minimum detectable electric field for this design is about 27 V/m, which is good but nearly a factor of 2 worse (in power density) than the suspended sphere configuration. The lower cut-off frequency is about 15–20 GHz.

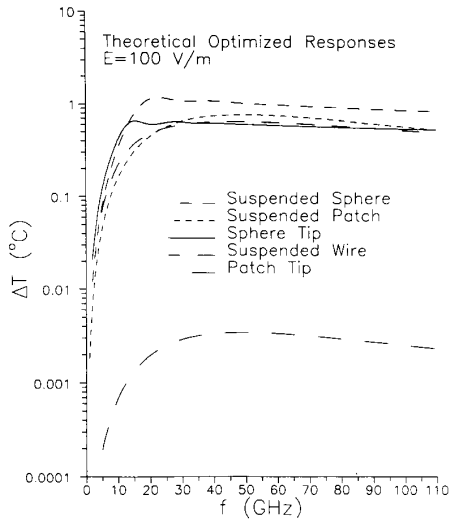

Fig. 5. Comparison of calculated frequency responses for optimized probes of the different designs.

TABLE I
OPTIMIZATION RESULTS FOR FIVE TO DESIGNS

Design	Optimized Parameters	E_{min}(V/m)	f_{min}(GHz)
Suspended sphere	r = 2 mm, σ = 10 S/m	21	15
Suspended patch	L = 2 mm, w = 0.5 mm, $(\sigma t)^{-1}$ = 209 Ω	25	20
Sphere tip	r = 3 mm, σ = 15 S/m	27	10
Suspended wire	L = 2 mm, a = 0.143 mm, σ = 30 S/m	27	15-20
Patch tip	L = 2 mm, w = 0.5 mm, $(\sigma t)^{-1}$ = 209 Ω	365	20

C. Comparison

In Fig. 5, we compare the calculated optimized responses for the different designs, and in Table I we collect the sensitivities and approximate lower frequency cutoffs. The suspended patch results are those obtained assuming a phosphor substrate that is 1 μm thick or less. Except for the patch tip design, all are predicted to be sufficiently sensitive to be of potential use. Of the four promising designs, the suspended sphere has the best predicted response. The other three are comparable to each other, with the suspended patch having a slightly greater sensitivity than the other two and the sphere tip having a better low-frequency cutoff. Because of uncertainties and approximations in the calculations, as well as anticipated difficulties in achieving the optimal conductivities required to produce the curves of Fig. 5, the differences among the suspended patch, sphere tip, and suspended wire designs are not considered very significant.

In deciding which of the TO designs to pursue further, we considered difficulty or feasibility of fabrication in addition to sensitivity and frequency response. For the suspended patch design, a stable 1-μm-thick phosphor substrate would require substantial development effort, if indeed it is even possible. Use of a thicker substrate (25–50 μm) reduces the response to about 0.4 times the prediction of Fig. 5, and even such a phosphor substrate would require some development. The sphere tip design is the easiest to fabricate, and in fact, such probes have been constructed for use at lower frequencies, for example, to map field intensity within a microwave oven [17]–[19]. We have therefore chosen to further investigate the suspended sphere design and the sphere tip design—the former because it promises the greater sensitivity and the latter because of its relative ease of fabrication.

IV. MEASUREMENTS

A. Description

Several probe tips of the resistive sphere designs were obtained. Most were of the sphere tip design, but we also obtained two of the suspended sphere design. The tips varied in size and composition. All the tips were tested, but we will present full sets of results for only three of the tips: two of the sphere tip design and one suspended sphere. For the suspended sphere and one of the sphere tips, the material used for the resistive sphere was carbon mixed in a resin binder. For the other sphere tip, the "tin-tip" tin oxide in a potassium silicate binder was used. The carbon sphere tip had a 0.99-mm-radius carbon sphere surrounding the phosphor tip, as in Fig. 1(c). The tin oxide sphere tip had a radius of 1.5 mm. It was enclosed in a hollow cylindrical casing of polycarbonate, as is depicted in Fig. 6(a). A normal, uncoated temperature sensor was also located within the casing to measure the ambient temperature. For the suspended sphere design, a carbon sphere of about 1 mm radius was supported by a very thin quartz fiber that passed through the sphere and was attached on either side to small polycarbonate posts. The entire assembly was surrounded by a polycarbonate casing (see Fig. 6(b)). This casing was in the form of a hollow cylinder with endcaps with the sphere and sensing fiber inside. A second fiber with an uncoated phosphor tip to measure the ambient temperature was also inside this casing. The two fibers entered through one of the endcaps along the axis of the cylinder.

Tests were performed in the NIST anechoic chamber to measure the heating of the tips when exposed to a known electric field. The measurements were all performed in the far field of the transmitting horns so that the incident field was a single free-space plane wave. We will therefore refer either to the incident electric field or power density, with the understanding that they are related by $E = 61.4\sqrt{P}$, where E is in volts per meter and P is in milliwatts per square centimeter. We shall describe the setup for the carbon sphere tip first and then note differences for the tin oxide and suspended sphere measurements. On the basis of past experience and preliminary tests, it was deemed desirable to enclose the carbon sphere tips in some electromagnetically transparent material such as foam in order to shield them from drafts in the anechoic chamber. A block of closed-cell foam containing a cavity was constructed for this purpose, but comparison of measurements on coated and uncoated tips, inside and outside the block, indicated that for very high field levels, the block itself was being heated and was in turn heating the probes. Therefore, a thin-walled box was built of

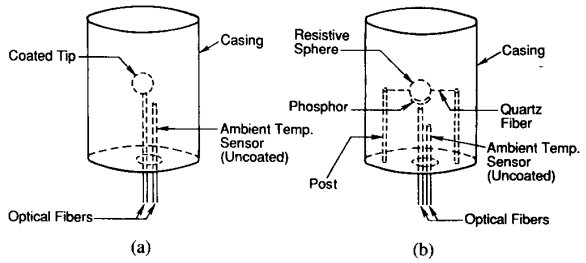

Fig. 6. Sketch of the (a) tin oxide and (b) suspended sphere probes used in the measurements.

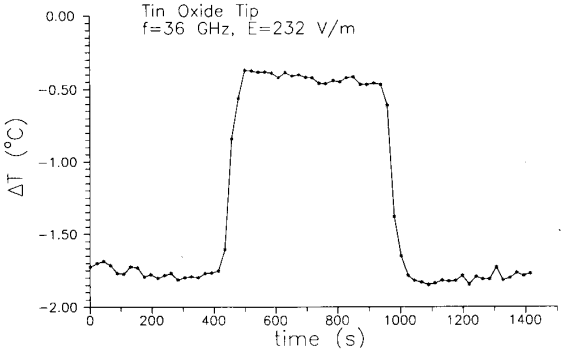

Fig. 7. Measured time dependence of difference in temperature between active and ambient sensors for the tin oxide sphere tip. The field was turned on at 414 s and was turned off at 937 s.

the same foam, and this configuration provided shielding without extraneous heating.

Two sensors were used in all the measurements: one with the carbon sphere tip, which was supposed to register a temperature rise in response to an applied electromagnetic field, and one ordinary uncoated tip to monitor the ambient temperature within the box. Both sensors were oriented with their fibers perpendicular to the electric field. The magnitude of the change in the difference between the readings of the two sensors should indicate the strength of the applied field. Data acquisition software was written to read the output of the two sensors, average over a number of samples, and compute the statistical uncertainty of the average ($s/\sqrt{N}$) in the set of samples for each sensor. It also computes the difference in the readings of the two sensors, again obtaining the average and uncertainty for the given number of measurements. In this manner, we can monitor the response of the field and ambient sensors individually, as well as their difference. By averaging over sets of 150 samples in all the measurements, we were able to achieve statistical uncertainties of about 0.02°C in the difference between the two sensors. (The time required for a set of 150 measurements was about 21 s.) We therefore take 0.04°C to be our minimum detectable temperature rise. In all the measurements, the readings were allowed to stabilize within about 0.02°C before the field was turned on, while it was on, and after it was turned off.

The foam box was not needed for the tin oxide or suspended sphere probes since the polycarbonate cylinder serves to protect the sensors from drafts. The ambient sensor was also already in the cylinder; therefore, no extra uncoated sensor was needed. Otherwise, the setup and procedures were the same for the tin oxide and suspended sphere probes as they were for the carbon sphere probe.

B. Results

Measurements were made from 12.5 to 40 GHz, generally at 2-GHz intervals, except for the suspended sphere, which was tested only from 18 to 40 GHz. At most frequencies, the incident electric field used was close to the maximum available at that frequency. The electric fields ranged from 130 to 540 V/m. At 36 GHz, the response as a function of power density was measured for each probe tip.

The time dependence of the response is shown in Fig. 7 for the tin-tip probe at 36 GHz and $E_{\text{inc}} = 232$ V/m. The times at which the field was turned on and off were 414 and 937 s, respectively. The vertical scale is the difference in temperature between the coated and uncoated tips at a given time. The time taken for each reading was about 21 s, and the response time is seen to be about 85 s. In the remainder of this section, the quantity of interest will be the change in the difference between the readings of the two probes, i.e., the rise in Fig. 7 when the field is turned on. This is determined by averaging the ten readings immediately before the field is turned on together with the first ten readings after the temperature has stabilized and after the field is turned off. This baseline value is then subtracted from the average of the ten readings immediately before the field is turned off to get the ΔT (or the "response") to which we refer in what follows.

The quantities of most interest are the magnitude and the frequency dependence of the response of each probe. These are shown in Fig. 8 for an incident field of 100 V/m. As noted above, the measurements were not actually done at 100 V/m. The results shown in Fig. 8 were obtained by scaling the measured results with the assumption that the response is proportional to the incident power density $\propto E_{\text{inc}}^2$. (This will be justified below.) The most important feature of Fig. 8 is the performance of the tin-tip probe. Its response is the best of the probes measured, and its frequency response is flat for frequencies of 30 GHz and above. From the measured response and the fact that the minimum detectable ΔT is 0.04°C, we infer that the minimum detectable electric field for the tin-tip probe is about 38 V/m. Since that is sufficiently sensitive to be useful as a transfer standard and since we can still improve the probe further, that is a very encouraging result.

There are several other features to note about Fig. 8. Neither the carbon tip nor the suspended sphere response has flattened by 40 GHz. That is to be expected since they are considerably smaller than the tin tip, and therefore, their operating plateau should begin at a higher frequency. Also as expected, the suspended sphere is more sensitive than the sphere tip of the same size and composition. Since neither probe's response has flattened yet, it is impossible to say exactly how much more sensitive the suspended sphere is, but it appears to be a factor of about 2. The tin sphere tip is more sensitive than the carbon sphere tip due to the greater

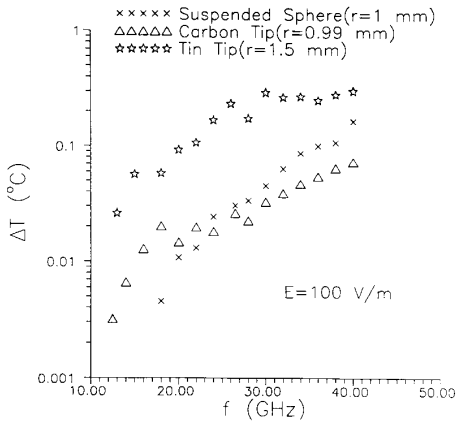

Fig. 8. Measured responses of three probe tips as functions of frequency.

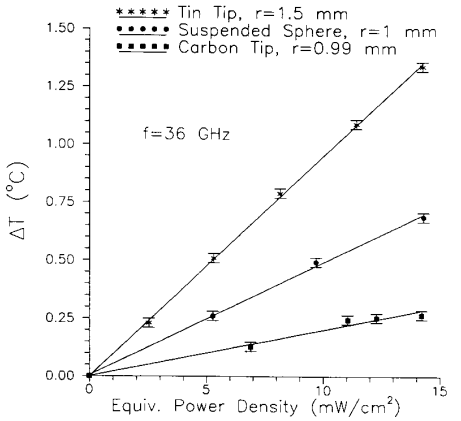

Fig. 9. Measured linearities of three probe tips at 36 GHz. Lines are best fit straight lines.

size of the tin tip, but that accounts for only part of the difference. Therefore, the material of the tin sphere tip must have a better (for present purposes) conductivity than does the carbon tip. This is a useful piece of information since we cannot directly measure the conductivity for these materials at these frequencies.

The linearity of each probe was tested at 36 GHz, and the results are shown in Fig. 9. The lines through the data points are the best fits to straight lines for the three probes. The linearity of each probe is clearly very good over the range measured. The error bars are our nominal ±0.02°C statistical uncertainty. A more detailed, point-by-point evaluation of the uncertainty would yield somewhat smaller uncertainties, but that does not seem warranted at this time.

An additional piece of information or test of our calculations can be obtained by comparing the frequency responses of two probe tips which differ only in size. We measured the response of two carbon sphere tips with radii of 0.625 and 0.91 mm from 12.5 to 18 GHz (see Fig. 10). The predicted dependence on sphere radius is given by (6). For the frequencies and dimensions of these measurements, the absorbed power is approximately proportional to r^3. Therefore, ΔT should be proportional to r^3 if conduction by the fiber is the

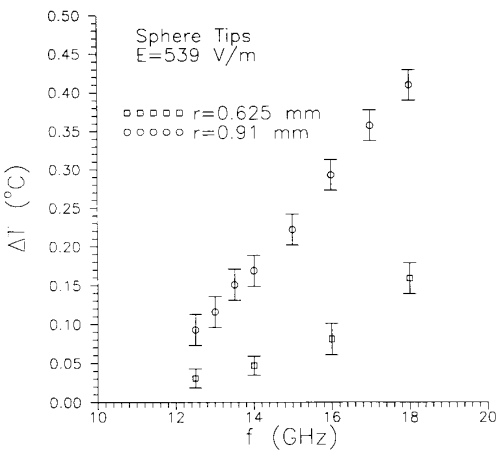

Fig. 10. Responses of two sphere tip probes differing only in radius.

dominant heat-loss mechanism for the carbon sphere, whereas if most of the heat is lost to the surrounding air, ΔT should vary as r^1. Using our approximate values for h and k_f, we expect that about 5 times as much heat should be lost to the fiber as is lost to the air (for the larger sphere). If we assume that ΔT is proportional to a power of r, $\Delta T \propto r^\alpha$ and combine the values and uncertainties of α for the four different frequencies measured, then our best value for α is 2.8 ± 0.3. This is consistent with all the heat being lost to the fiber but does not preclude some heat loss to the air. To estimate the relative amounts of each, we write ΔT as

$$\Delta T = r^3 a(f)/(1 + br^2) \tag{8}$$

where br^2 is the amount of heat lost to the air relative to that lost to the fiber for a sphere of radius r, and $a(f)$ is some function of frequency. For the larger carbon tip ($r = 0.91$ mm), we obtain $br^2 = -0.1 \pm 0.2$, indicating that while most of the heat is lost to the fiber, as much as 10–20% could be lost to the air. This is in approximate agreement with our expectations. The practical importance is twofold. It indicates that the sensitivity of the design can be increased significantly (for $r = 1 - 2$ mm) by reducing the thermal contact between sphere and fiber. That, of course, is the point of the suspended sphere design. It also indicates that as the size of the sphere becomes larger, heat loss to the fiber decreases in importance, and reductions in thermal contact between sphere and fiber pay smaller dividends.

C. Comparison to Theory

A direct comparison of theory and experiment for the magnitude and frequency dependence of the response is not possible because we do not know the conductivities of the resistive spheres. We therefore computed the responses for various values of conductivity (σ) ranging from 1 to 10^5 S/m. For the tin tip, the theoretical responses are roughly the same size as the measured results for values of σ from 20 to 200 S/m, as is shown in Fig. 11. Because of the uncertainty in the values of various parameters, agreement within a factor of 2–5 is all one can expect. There is, however, no value of σ for which the theoretical results can match the

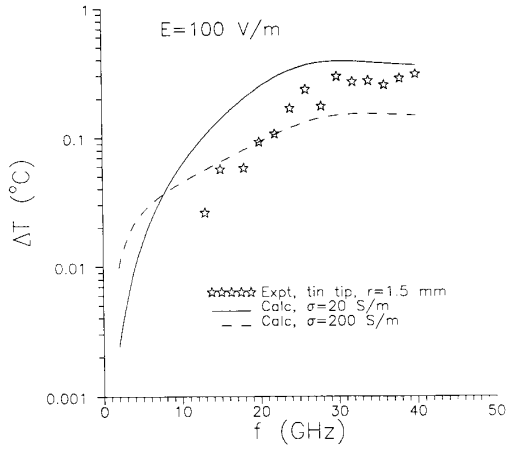

Fig. 11. Comparison of calculated and measured responses of tin oxide sphere probe.

steep slope of the data, and the slope depends only on σ and on r, which is known well. The steep slope of the data could be due to a variation of σ across this frequency range, but it seems unlikely that σ could vary rapidly enough (and that it would then suddenly become constant again). A more plausible explanation is that the fiber and phosphor in the sphere reduce its effective radius. That would shift the predicted curve to the right, resulting in a steeper predicted slope in the frequency range measured. Analogous results are obtained for the other two probe tips.

V. Comments and Conclusions

The test results described above are very encouraging in that they demonstrate the viability of the thermo-optic probe design. In addition, they and the calculation results point to possible improvements we can make on the probes. The biggest and easiest improvement would be to use a larger resistive sphere. Our calculations indicated that the optimal radius would be about 3 mm. That could increase the sensitivity by a factor of almost 2, and it would also lower the frequency at which the response becomes flat, down to between 15 and 20 GHz.

Other possible areas of improvement would be to reduce the thermal contact between sphere and fiber and to use a better (not necessarily larger) conductivity. It is not clear that much could be gained in these areas, however. For larger spheres, heat loss to the fiber decreases in importance. As for the conductivity, the response is not especially sensitive to moderate (factors of a few) changes in the conductivity, and we cannot really measure the conductivity at millimeter wave frequencies anyway. Additional sensitivity could also be obtained by using an upgraded version of the metering unit for the temperature sensor, which is now available. The newer model is capable of sampling significantly faster than the one used in our measurements and could increase sensitivity by a factor of about 2 to 4.

Although the results thus far are encouraging, some potential problems remain. We have not yet tested the isotropy of any of the probes. Although the resistive sphere itself should be isotropic, the surrounding structure and the optical fibers obviously are not, and if they experience heating, it would degrade or destroy the isotropy. That could be acceptable for a transfer standard probe, but it is undesirable in hazard meter applications. In addition, there is the question of stability over a long time interval of continuous use. In the measurements, the field was on for about 10 min at a time. We have not yet tested the thermal stability of the probes for longer periods of time.

In summary, we have developed a design for microwave and millimeter-wave electric-field probes based on an optically sensed thermometer. We theoretically analyzed and evaluated numerous different configurations for the resistive element, and a resistive sphere was chosen as the most promising. Several probe tips of this design were obtained, and their sensitivity, frequency response, and linearity were tested. Results of these tests were very encouraging. In particular, one of the designs exhibited a flat frequency response above about 30 GHz with a sensitivity of 38 V/m and excellent linearity. This in itself constitutes adequate performance for a transfer standard for millimeter waves, but in addition, we anticipate significant improvements in both sensitivity and frequency response by using a larger resistive sphere. This and other improvements are now being pursued to optimize the probe.

Acknowledgment

The authors are very grateful to K. Wickersheim and M. Sun of Luxtron Corporation for numerous suggestions and discussions and for fabricating the probe tips used in the measurements.

References

[1] M. Kanda and L. D. Driver, "An isotropic electric-field probe with tapered resistive dipoles for broad-band use, 100 kHz to 18 GHz," *IEEE Trans. Microwave Theory Tech.*, vol. MTT-35, pp. 124–130, Feb. 1987.

[2] J. Randa, M. Kanda, and R. D. Orr, "Resistively-tapered-dipole electric-field probes up to 40 GHz," to be published in *Proc. IEEE 1991 Int. Symp. EMC* (Cherry Hill, NJ), 1991.

[3] J. Randa, M. Kanda, D. Melquist, and R. D. Orr, "Thermo-optic designs for microwave and millimeter-wave electric-field probes," in *Proc. IEEE 1989 Nat. Symp. EMC* (Denver), 1989, pp. 7–11.

[4] S. Hopfer, "The design of broad-band resistive radiation probes," *IEEE Trans. Instrum. Meas.*, vol. IM-21, pp. 416-421, Nov. 1972.
[5] E. Aslan, "Broad-band isotropic electromagnetic radiation monitor," *IEEE Trans. Instrum. Meas.*, vol. IM-21, pp. 421-424, Nov. 1972.
[6] S. Hopfer and Z. Adler, "An ultra broad-band (200 kHz-26 GHz) high-sensitivity probe," *IEEE Trans. Instrum. Meas.*, vol. IM-29, pp. 445-451, Dec. 1980.
[7] J. Randa and M. Kanda, "Multiple-source, multiple-frequency error of an electric-field meter," *IEEE Trans. Antennas Propagat.*, vol. AP-33, pp. 2-9, Jan. 1985.
[8] K. A. Wickersheim and M. H. Sun, "Fiberoptic thermometry and its applications," *J. Microwave Power,* vol. 22, no. 2, pp. 85-94, 1987.
[9] V. M. Martin, R. M. Sega, and R. Durham, "Fiber optic microwave power probe," *Optical Eng.*, vol. 26, no. 2, pp. 170-173, Feb. 1987.
[10] G. Mie, *Ann. Physik,* vol. 25, no. 4, p. 377, 1908.
[11] J. Stratton, *Electromagnetic Theory.* New York: McGraw Hill, 1941, ch. 9.
[12] M. Born and E. Wolf, *Principles of Optics.* New York: Pergamon, 1965, ch. 13.
[13] A. J. Chapman, *Heat Transfer.* New York: Macmillan, 1984, 4th ed.
[14] R. S. Elliot, *Antenna Theory and Design.* Englewood Cliffs, NJ: Prentice-Hall, 1981, ch. 7.12.
[15] R. W. P. King, *The Theory of Linear Antennas.* Cambridge, MA: Harvard University Press, 1956, ch. 1.
[16] E. C. Jordan and K. G. Balmain, *Electromagnetic Waves and Radiating Systems.* Englewood Cliffs, NJ: Prentice-Hall, 1968, ch. 14.
[17] K. A. Wickersheim, paper given at the 23rd Microwave Power Symposium, Ottawa, Canada, Aug. 1988.
[18] K. A. Wickersheim, M. H. Sun, and A. Kamal, "A small microwave E-field probe utilizing fiberoptic thermometry," *J. Microwave Power,* vol. 25, no. 3, pp. 141-148, 1990.
[19] J. Randa, "Theoretical considerations for a thermo-optic microwave electric-field-strength probe," *J. Microwave Power,* vol. 25, no. 3, pp. 133-140, 1990.

James Randa (M'89) received the Ph.D. degree in physics from the University of Illinois, Urbana, in 1974. He then successively held postdoctoral or faculty positions at Texas A&M University, University of Manchester (England), and the University of Colorado, Boulder.

During this time, he did research on the phenomenology of elementary particles and on theories of fundamental interactions. Since 1983, he has been with the Electromagnetic Fields Division of the National Institute of Standards and Technology, Boulder, CO, where he has worked on characterization of electromagnetic environments, probe development, and other topics in EMI metrology.

Motohisa Kanda (F'88) was born on September 10, 1943 in Kanagawa, Japan. He received the B.S.E.E. degree in 1966 from Keio University, Tokyo, the M.S.E.E. degree in 1968, and the Ph.D. degree in 1971 from the University of Colorado, Boulder.

From 1965 to 1966, he was a Research Technician at Keio University, where he did research on the avalanche breakdown in the germanium p-n junction at a cryogenic temperature. From 1966 to 1971, he was a Research Assistant at the University of Colorado, where he conducted research on impact ionization of impurities in n-type germanium and nonreciprocal behavior in a solid-state plasma at millimeter and submillimeter wavelengths. In 1971, he joined the staff of the Electromagnetic Fields Division, the National Institute of Standards and Technology (formerly Bureau of Standards), Boulder, CO, where he is currently leader of the Fields and Interference Metrology Group. Concurrently, he serves as a professor adjunct in the Electrical and Computer Engineering Department of the University of Colorado, Boulder.

Dr. Kanda is Editor of the IEEE TRANSACTIONS ON ELECTROMAGNETIC COMPATIBILITY and chairman of Commission A of the International Union of Radio Science. He has received the Bronze Medal (1981) and Silver Medal (1989) from the Department of Commerce. He has received two IEEE EMC Transaction Best Paper Awards in 1982 and 1989 and other numerous awards from the IEEE EMC Society and the Department of Commerce.

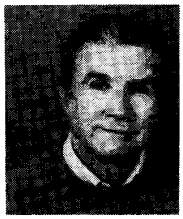

R. David Orr received the B.S. degree from Kalamazoo College, Kalamazoo, MI, in 1950, and the M.S. and Ph.D. degrees from the University of Colorado, Boulder, in 1960 and 1971, respectively, all in physics.

He worked as a heat treating engineer at the Western Electric Company, Cicero, IL, and continued as a Physicist in the Particle Accelerator Division of Argonne National Laboratory, Lemont, IL. After several years in a nutrient matrix of Army service, graduate school, science journalism, and teaching physics at San Jose State College, San Jose, CA, he emerged in 1979 as a Physicist at the National Bureau of Standards, Boulder, CO. His current assignment is to evaluate the pyramidal horns and anechoic chamber employed by NBS to establish standard radio-frequency fields in which calibrations and electromagnetic susceptibility measurements are made.